Ultrathin Polymeric Interpenetration Network with Separation Performance Approaching Ceramic Membranes for Biofuel

Lan Ying Jiang
Nanoscience and Nanotechnology Initiative, National University of Singapore, Singapore 117576

Hongmin Chen and Yan-Ching Jean
Dept. of Chemistry, University of Missouri-Kansas City, Kansas City, MO 64110

Tai-Shung Chung
Dept. of Chemical and Biomolecular Engineering, National University of Singapore, Singapore 119260

DOI 10.1002/aic.11652
Published online December 4, 2008 in Wiley InterScience (www.interscience.wiley.com).

Biofuel has emerged as one of the most strategically important sustainable fuel sources. The success of biofuel development is not only dependent on the advances in genetic transformation of biomass into biofuel, but also on the breakthroughs in separation of biofuel from biomass. The "separation" alone currently accounts for 60–80% of the biofuel production cost. Ceramic membranes made of sophisticated processes have shown separation performance far superior to polymeric membranes, but suffers fragility and high fabrication cost. We report the discovery of novel molecular engineering and membrane fabrication that can synergistically produce polymeric membranes exhibiting separation performance approaching ceramic membranes. The newly discovered Polysulfone/Matrimid composite membranes are fabricated by dual-layer coextrusion technology in just one step through phase inversion. An ultrathin dense-selective layer made of an interpenetration network of the two materials with a targeted and stable interstitial space is formed at the interface of two layers for biofuel separation. The combined molecular engineering and membrane fabrication approach may revolutionize future membrane research and development for purification and separation in energy, environment, and pharmaceuticals. © 2008 American Institute of Chemical Engineers *AIChE J*, 55: 75–86, 2009

Keywords: biofuel, purification and separation, membranes, dehydration, in-situ interpenetration networking

Introduction

Energy is a major concern globally because of resource depletion and record higher prices for oil. Among many energy alternatives, biofuel, hydrogen, natural gas, and

Correspondence concerning this article should be addressed to T.-S. Chung at chencts@nus.edu.sg.

syngas (synthesis gas) may likely emerge as the four strategically important sustainable fuel sources in the foreseeable future. Within these four, biofuel is the most environmentally friendly energy source because of the concerns of exhausted green house gases from petroleum-derived fuels.[1] Biofuel generally includes methanol, ethanol, butanol isomers, and biodiesel. However, the success of biofuel development is not only dependent on the novel biological discovery in genetic transformation of biomass into biofuel, but also on engineering breakthroughs in the separation of biofuel from biomass because the "separation" alone currently accounts for 60–80% of the overall cost.[2]

Since biofuel is derived from biomass, multistep separations and purifications must be conducted to first remove small molecular weight biomass and then to separate biofuel from water. These bioproducts are labile and heat sensitive; athermal separation processes must be used. The removal of small molecular weight biomass can be done effectively by ultrafiltration and nanofiltration membranes, whereas the separation of biofuel from water is scientifically challenging. Yet the membrane-based pervaporation technology has demonstrated incomparable efficiency in separating azeotropic, close boiling point and heat sensitive mixtures compared to other separation technologies (e.g., distillation, extraction, and crystallization). In pervaporation, the feed of aqueous biofuel mixture contacts with one side of a nonporous membrane and the permeated product is collected from the other side under lower pressures. Separation occurs because of preferential sorption and transport through the membrane.

There are two types of membranes competing for the dehydration of biofuel; namely inorganic ceramic and polymeric membranes.[3] Figure 1 compares their separation performance for biofuel mixtures comprising water and 2-methyl-2-propanol (tert-butanol) tested at industrial operation conditions of 80°C and a feed water concentration range from 20 wt % to less than 5 wt %.[4–7] Butanol is chosen as the target because it is superior to ethanol for its higher energy density and burnable in conventional turbofan engines.[8] Polymeric membranes are currently far inferior to inorganic membranes, especially in terms of flux. The origins of performance disparity arise from their differences in interstitial chain space, dense-selective thickness and molecular interactions with the feed penetrants. The solution-diffusion mechanism is widely accepted for pervaporation membranes.[9,10] The permeability coefficient P is given by the product of diffusivity D and solubility S:

$$P = DS$$

For a binary biofuel system consisting of water (A) and butanol (B), ceramic membranes have higher diffusion selectivity, (D_A/D_B), than polymeric membranes because the former has fixed interstitial space for diffusion jump whereas the latter fluctuates because of thermal motions of the segments of polymer chains. In addition, zeolite- and silica-based ceramic membranes may have greater sorption selectivity (S_A/S_B) than most polymeric membranes owing to the former having better interactions with water than the latter.

Here, we report hollow fiber membranes that can exhibit extremely high separation performance far surpassing the prior art of polymeric membrane and approaching ceramic

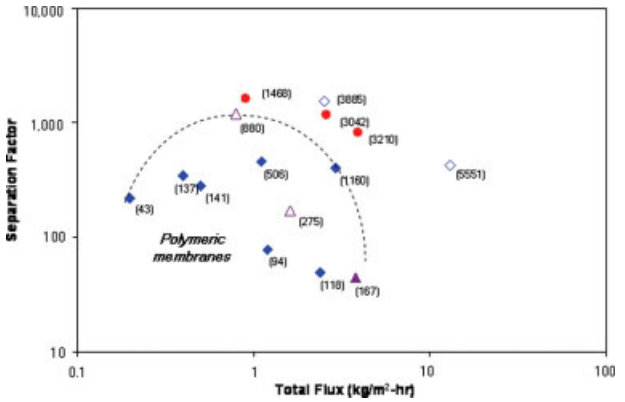

Figure 1. Plot of literature data for tert-butanol dehydration by pervaporation-separation factor vs. total flux.

●, Dual-layer hollow fiber in current work; ◇, inorganic membranes (4–5); ◆, polymeric membranes (6–7); △, Polysulfone single-layer hollow fiber in current work; ▲, Matrimid single-layer hollow fiber in current work. Note: Feed water concentration ranges from 2.2 to 17 wt %; operation temperature 80°C; the data in the parentheses is pervaporation separation index (PSI) (PSI = flux × separation factor and is usually used to characterize the performance of the pervaporation process). [Color figure can be viewed in the online issue, which is available at www.interscience.wiley.com.]

membranes in 2-methyl-2-propanol (tert-butanol) dehydration. They have an ultrathin dense-selective layer made of a miscible blend with a targeted and much stable interstitial space at the interface of two layers within the membrane cross-section. As can be seen in Figure 1, the overall performance, especially the flux of the polymeric hollow fibers in this study is significantly higher than those of commercially available polymeric membranes.[6,7] Compared with the best inorganic membrane (e.g., PERVAP® SMS of microporous silica), the flux of the dual-layer hollow fibers is lower, whereas the selectivity is higher. The pervaporation separation index (PSI) (PSI = flux × separation factor) reconfirms that the dual-layer hollow fibers are not only superior to other polymeric membranes, but also approaches the best ceramic membranes in terms of the overall separation property.[4,5] These newly discovered membranes are fabricated by dual-layer coextrusion technology in just one step through a phase inversion process. Central to this performance achievement is the synergy of unique pair of miscible polymeric blends with the aid of controlled intermolecular diffusion by means of molecular engineering and membrane fabrication.

Experimental

Materials

Udel® Polysulfone (PSf) from Solvay and Matrimid® 5218 (Matrimid) from Ciba (Hawthorn, New York) were the polymers used in this study; the chemical structure of the two polymers are shown in Figure 2. Table 1 summarizes overview of the band assignments and wavenumbers of the two polymers. The polymers were dried in a vacuum oven at 110–120°C for overnight before dope preparation; *N*-methylpyrrolidinone (NMP) from Merck was used as the solvent.

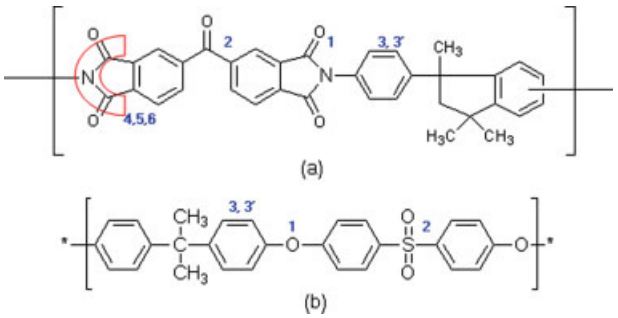

Figure 2. Chemical structures of (a) Matrimid and (b) Polysulfone.

The numbers correspond to the numbers in Table 1. [Color figure can be viewed in the online issue, which is available at www.interscience.wiley.com.]

Ethanol from Merck was used as a nonsolvent. Methanol from Merck and hexane from Fischer were used for solvent exchange. Tert-butanol for the pervaporation dehydration experiment was supplied by Fischer. The solubility parameters of the materials and chemicals involved in the pervaporation is summarized in Table 2.

Dope and bore fluid preparation and hollow fiber spinning

The homogeneous polymer solutions were prepared according to the following procedure. The solvent or solvent/nonsolvent mixture was first stirred at 0–5°C in an ice bath, followed by the addition of a desired amount of polymer; then the temperature gradually increased to room temperature as the ice melted. The solutions were agitated with the Eurostar power-control stirrer at high speed for at least 24 h for the polymer to dissolve completely and homogeneously. Table 3 shows the compositions of dopes and bore fluid for the dual-layer hollow fibers.

The details about single and dual-layer hollow fibers spinning system have been described in Wang et al.'s work.[14] The polymer solutions were degassed 24 h before loading into two individual syringe pumps (ISCO 500D) followed by another 24 h degassing after loading. Tap water was used as the external coagulant with a temperature of 25°C. The hollow fibers were spun by extrusion of the polymer solutions/solution and bore fluid simultaneously out of the dual-layer or single-layer spinneret orifice and subsequent phase inversion of nascent fibers in a water coagulant bath. The spinning conditions and parameters are summarized in Table 3. The as-spun fibers were rolled up by a drum, and then cut into segments before being rinsed in a clean water bath for at least 5 days to remove the remaining NMP. Solvent exchange was then carried out by first soaking the fibers into methanol three times, each session 30 minutes, then repeating the same procedure but this time with *n*-hexane. After being taken out from the hexane, the fibers were air-dried at room temperature, thereafter they were heat treated at 75°C under vacuum for 3 h.

Table 1. Overview of Band Assignments and Wave Numbers for IR Spectrum of Neat Matrimid and Polysulfone

Number	Wave Number (cm^{-1})	Band Assignment
(A) Matrimid		
1a	1772	C=O symmetric stretch
1b	1715	C=O asymmetric stretch
2	1666	C=O stretch of benzophenone carbonyl
3 and 3′	1484 and 1508	Aromatic skeleton vibration
4	1364	C−N−C axial stretch
5	1092	C−N−C transverse stretch
6	719	C−N−C out-of-plane bending
(B) Polysulfone		
1 and 1′	1014 and 1236	C−O−C stretching vibration
2a	1148	S=O symmetric vibration
2b	1292	S=O asymmetric vibration
3 and 3′	1484, 1508, and 1584	Aromatic stretching and aromatic skeleton vibration

Table 2. Comparison of the Solubility Parameters*

	δ_d $(Mpa)^{1/2}$	δ_p $(Mpa)^{1/2}$	δ_h $(Mpa)^{1/2}$	δ_{sp} $(Mpa)^{1/2}$
H_2O†	15.6	16.0	42.3	47.8
Ethanol‡	18.2	10.1	20.1	28.9
tert-Butanol‡	17.7	6.1	15.7	24.4
NMP‡	16.8	12.1	8.7	22.5
Matrimid‡	18.7	9.5	6.7	22.1
Matrimid§	/	/	/	23.9
Polysulfone‡	18.2	2.5	7.3	19.7
Polysulfone¶	17.8	11.0	7.0	22.1
Polysulfone§	/	/	/	21.9

*δ_{sp}, solubility parameter; δ_d, dispersion force; δ_p, polar force; δ_d, hydrogen bonding.
†Ref. 11
‡Calculated using the method from Ref. 12.
¶Adapted from Ref. 13.
§Calculated using Acceryls Material Studio.

Module fabrication and pervaporation test

The fibers were fabricated into hollow fiber modules with feed from the shell side. The holder for a module consisted of two Swagelok® stainless steel male run tees connected by PFA tubing. One piece of fiber was pulled through the inner channel of the holder. Both ends of the module (male run tees) were sealed with slow cure epoxy. After 24 h for the epoxy to get cured, the modules were mounted on the pervaporation system for testing. The effective length of the fiber in contact with the feed solution was around 15 cm.

The schematic of pervaporation apparatus for the characterization of hollow fiber membranes is given in Figure 3. Briefly, hollow fiber modules were mounted onto the pervaporation system with shell side as the feed side and lumen side as the permeate side. At least two modules with same fabrication and conditions were examined for each pervaporation condition. Two liters of tert-butanol/water mixture was used as the feed solution. The recirculation rate was set at 30 L/h-module. The pressure at the permeate side was normally maintained at less than 0.5 kPa. The feed temperature was maintained at 80°C. The system was stabilized for 2 h before the collection of samples. According to the observation in previous and this study, 2 h were enough for both flux and composition of permeate to reach a stable state, especially for hollow fibers with a thin skin layer. Permeate samples were collected by a cold trap immersed in liquid nitrogen at 0.5–1 h interval for at least 5 h. The samples were weighted

Table 3. Hollow Fiber Fabrication Conditions

(A) Dope/Bore Fluid Compositions

Layer	Polymer*	Solvent (Weight Ratio)		Polymer Concentration (wt %)	Dope Viscosity (cp)
Outer	Polysulfone	NMP	(/)	36.9	126930
Inner	Matrimid	NMP/EtOH	(4/1)	22.8	56828
Bore	/	NMP/water	(95/5)	/	/

(B) Spinning Conditions

Fiber ID†	Air Gap (cm)	Take Up Rate	Dope Flow Rate (cc/min)		
			Outer Layer	Inner Layer	Bore Fluid
P/M-A	1	Free draw	0.12	0.8	0.3
P/M-B	1	Free draw	0.08	0.8	0.3
P/M-C	1	Free draw	0.06	0.8	0.3

*Udel® Polysulfone from Solvay and Matrimid® 5218 from Ciba polymers.
†P/M-dual-layer hollow fiber with Polysulfone outer layr and Matrimid inner layer.

by a Mettler Toledo balance. The sample compositions were analyzed with three parallel injections by a Hewlett-Packard GC 6890 with a HP-INNOWAX column (packed with cross-linked polyethylene glycol) and a TCD detector. Finally, the data of flux and composition were averaged. The feed content varied less than 1 wt % during the entire experiment and therefore was considered as constant during the experiment because of the large quantity of feed solution comparing to the permeate sample. Flux and separation factors were calculated by the following equations:

$$J = \frac{Q}{At} \tag{1}$$

$$\alpha_{2/1} = \frac{y_2/y_1}{x_2/x_1} \tag{2}$$

where, J is the flux, Q is the total mass transferred over time t, A the membrane area, x_2 and y_2 are the mole fractions of water in the feed and permeate, respectively, and x_1 and y_1 are the mole fractions of alcohol in the feed and permeate, respectively. The driving force for pervaporation can be expressed as a vapor pressure difference. The basic pervaporation transport equations based on the solution diffusion model are[15]:

$$J_i = \frac{P_i}{l}\left(p_i^{\mathrm{f}} - p_i^{\mathrm{p}}\right) = \overline{P}_i\left(p_i^{\mathrm{f}} - p_i^{\mathrm{p}}\right) \tag{3}$$

where P_i is the membrane permeability, which is the product of the solubility and diffusivity. Superscripts f and p correspond to the feed and permeate; l is the membrane dense-layer thickness; p denotes the partial vapor pressure, whereas

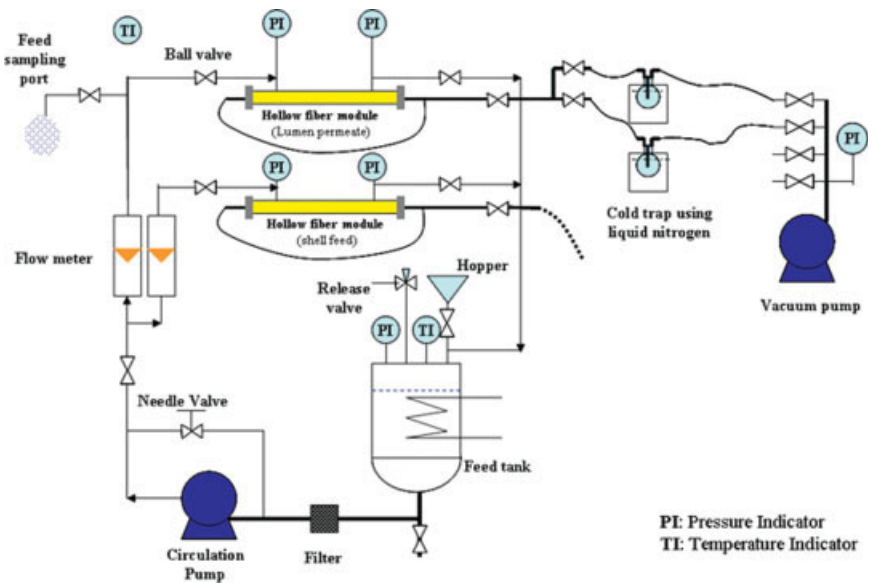

Figure 3. Schematic of hollow fiber pervaporation separation system.

[Color figure can be viewed in the online issue, which is available at www.interscience.wiley.com.]

$\overline{P}_i$ is the permeance. The membrane selectivity β is defined as $\overline{P}_2$ divided by $\overline{P}_1$.

The partial vapor pressure (fugacity) of each component on the feed side can be calculated based on its concentration in the feed liquid mixture:

$$p_i^{\mathrm{f}} = x_i \gamma_i p_i^{\mathrm{s}} \tag{4}$$

where the superscript s indicates the saturated state and γ is the activity coefficient. In this study, p_i^{s} and γ_i were obtained from the HYSYS DISTIL software (version 5.0, provided by Hyprotech Ltd., Canada). Substituting Eq. 4 in Eq. 3, we can have permeance based on the following equation[6–7,16]:

$$\overline{P}_i = \frac{J_i}{x_i \gamma_i p_i^{\mathrm{s}} - p_i^{\mathrm{p}}} \tag{5}$$

From our previous experience with pervaporation by hollow fibers, it has been found that the fiber performance and stability was quite sensitive to the down stream vacuum status. When the permeate vapor could not be sucked away from the lumen channel very quickly and accumulated in the permeate side, the fiber performance would somewhat deteriorate. This is probably because of the intensified swelling by the condensed permeate in the membrane. In consideration of this, a standby cold trap adopted in many other works was also used to keep the permeate side in a continuous vacuumed state even during sample collection.[17] Additionally, the samples were usually collected every half an hour for fibers with much higher flux. After testing of one feed with certain composition and before testing another batch of feed solution, the fiber was immediately dried with air purge from shell side and vacuum in the lumen side. The fiber thus treated could be used repeatedly. The permeate flux and composition as a function of time in the dehydration of 86 wt % tert-butanol aqueous solution are displayed in Figure 4. It can be safely concluded that fibers P/M-A, B, and C perform stably during the continuous testing of at least 5 h when the operation complies with above procedures.

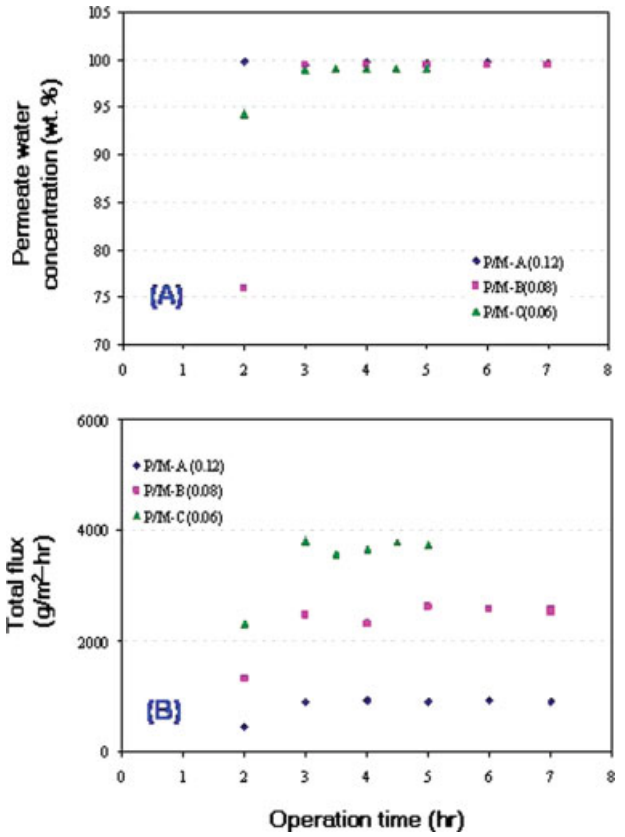

Figure 4. Performance of Polysulfone/Matrimid dual-layer hollow fibers as a function of operation time.

Feed: 86/14 tert-butanol/water by weight; final temperature 80 °C; flow rate of feed mixture: 30 L/h for one module. [Color figure can be viewed in the online issue, which is available at www.interscience.wiley.com.]

Membrane characterization

Field-emission scanning electron microscopy (FESEM JEOL JSM-6700LV) was applied to observe the membrane morphology. X-ray photoelectron spectroscopy (XPS) measurements were carried out by an AXIS Hsi spectrometer (Kratos Analytical Ltd., England) using the monochromatized Al K X-ray source (1486.6 eV photons) at a constant dwell time of 100 ms and a pass energy of 40 eV. All core-level spectra were obtained at a photoelectron take-off angle of 90° with respect to the sample surface. X-ray energy dispersive spectrometry (EDX) elemental mapping was taken using an Oxford INCA energy dispersion of X-ray system equipped with a super ultrathin window (SUTW) connected to a SEM JEOL JSM-5600LV operating at 15 kV. The glassy transition temperatures of dual-layer hollow fibers were measured using a Perkin-Elmer differential scanning calorimeter (DSC) Pyris 1 with heating and cooling rates of 20°C/min and N_2 purging of 20 mL/min. An attenuated total reflection ATR-FTIR (Perkin-Elmer FTIR spectrometer) was used to examine the degree of chemical cross-linking with a scan number of 16. An X-ray diffractometer (GADDS XRD system, Bruker AXS) was performed to quantitatively measure the ordered dimension and interchain spacing of polymer phase and the structure of zeolites at room temperature. Ni-filtered Cu Kα with a radiation wavelength λ = 1.54 Å was used at 40 kV and 40 mA.

Positron annihilation lifetime spectroscopy measurements

The positron annihilation lifetime spectroscopy (PALS) measurements were performed in nitrogen at ambient temperature using an automated EG&G Ortec fast-fast spectrometer. The timing resolution of the system was 240 ps. The polymer hollow fibers were packed tightly along the axis direction to form a thin film of several layers of hollow fibers running parallel to each other. The film has a thickness of 1 mm and surface area of 1.5 × 1.5 cm^2 on either side of a Na-Ti foil source. There was no source correction needed for the Ti foil (thickness 2.5 μm). Each spectrum consisted of ~10 million integrated counts. The spectra were modeled as the sum of three decaying exponentials or as a continuous distribution. The shortest lifetime, τ_1, was fixed at 0.125 ns, which is characteristic of *para*-positronium self-annihilation. The

Table 4. Pervaporation Performance of Polysulfone/Matrimid Dual-Layer Hollow Fibers as a Function of Outer Layer Dope Flow Rate During Fiber Spinning

	Total Flux (g/m^2-h)	Permeate Water Composition (wt %)	Separation Factor	Water Permeance (mol/m^2-h-kPa)	tert-Butanol Permeance (mol/m^2-h-kPa)	Selectivity
P/M-A	901	99.6	1529	1.24	0.0056	1631
P/M-B	2562	99.5	1100	3.48	0.022	1170
P/M-C	3853	99.2	822	5.41	0.046	859

Feed, 86/14 tert-butanol/water by weight; Final temperature, 80°C; Flow rate of feed mixture, 30L/hr per module.

second lifetime, τ_2, was ~0.35–0.45 ns for all samples, characteristic of free and trapped positrons. The longer lifetime, τ_3, was >1 ns and attributed to annihilations of *ortho*-positronium in the free volume elements of the polymer.

Results and Discussion

Pervaporation performance of the Psf/Matrimid dual-layer hollow fibers

Table 4 summarizes the averaged performance of the dual-layer hollow fibers with different PSf outer-layer dope flow rates for the dehydration of 86 wt % tert-butanol aqueous solution. The conventional parameters including flux and separation factor are given along with permeance and selectivity. It is apparent that the PSf outer layer dope flow rate can alter the hollow fibers separation properties significantly. The flux (permeance) augments by more than three folds from 0.9 kg/m^2-h (permeance 1.3 mol/m^2-h-kPa) to 3.9 kg/m^2-h (permeance 5.4 mol/m^2-h-kPa) when the outer layer dope flow rate changes from 0.12 to 0.06 mL/min. At the same time, the separation factor (selectivity) decreases slightly from ~1500 (selectivity = 1600) to ~820 (selectivity = 860). A further aspect worth noticing is that the dual-layer hollow fibers were only treated at 75°C for 3 h. In contrast to this mild post-treatment condition, high temperatures annealing were always applied to asymmetric hollow fibers or flat membranes in many other researches to acquire enough separation factors.[18–24]

Figure 1 has given a comprehensive overview of pervaporation data for tert-butanol dehydration presented in open literature, including the results of current work. For a fair comparison and for the determination of the most appropriate one for industrial applications, an operation temperature of 80°C and a feed water concentration range from 20 wt % to less than 5 wt % are chosen. A point that can be safely made is that the PSf/Matrimid dual-layer hollow fiber is promisingly bridging the gap between the previous polymeric membranes and inorganic membranes. Both the flux and the separation factor of the dual-layer hollow fibers in this study are noteworthily higher than other polymeric membranes even including the commercially available ones.[6,7] Compared with the best inorganic membrane shown in Figure 1 (e.g., PERVAP® SMS of microporous silica), the flux of the dual-layer hollow fibers is lower, whereas the separation factor higher. The PSI coefficients (PSI = flux × separation factor) reconfirm that the overall separation property of the PSf/Matrimid dual-layer hollow fibers is not only superior to other polymeric membranes, but also approaches the best ceramic membranes.[4,5]

Both single-layer Matrimid and PSf hollow fibers were fabricated under the same conditions from the same dope compositions. The single-layer Matrimid hollow fiber is fully porous without any separation properties, whereas the single-layer Psf hollow fibers have much inferior separation performance as also shown in Figure 1. Clearly, the newly developed dual-layer membranes propose an approach that synergistically combines the strengths of these two materials to produce excellent membrane for pervaporation.

Characterizations

FESEM Characterization of the Psf/Matrimid Dual-Layer Hollow Fibers. Figure 5 displays an example of the structure of the produced dual-layer hollow fiber membranes was studied by FESEM. Typically, the fibers have asymmetric structure and macrovoids are formed in both outer and inner layers. The PSf outer layer outer skins are seemingly dense (Figure 5a), whereas the Matrimid inner layer inner skins are fully porous (Figure 5c). The estimated thicknesses of the PSf outer layer changes from 20 to 15, and then 10 μm, when the outer-layer dope flow decreases from 0.12 to 0.06 mL/min. Figure 6 shows the cross-sections of the PSf outer layer and Matrimid inner layer, and the dense selective layer at the interface. The Matrimid inner layer was spun from a solution containing 61.6 wt % NMP and 15.4 wt % ethanol, whereas the PSf outer layer from a solution consisting of 63.1 wt % NMP. Both solutions have very similar solubility parameters (21.5 vs. 23.4 $Mpa^{0.5}$) but consist of different compositions. Once contacting with each other, the ethanol will move from the Matrimid solution to the Psf solution because of the great concentration difference; therefore, the polymer concentration at the outer skin of the Matrimid inner layer will become high enough to form a dense structure and solidify during the following solidification. This process may be called as delayed demixing.

In addition, Matrimid and Psf molecules will diffuse into each other because of close solubility parameters (Table 2) and high miscible tendency, which results in an ultrathin interpenetrated and miscible layer formed upon the Matrimid inner layer. After annealing at 75°C, a defect-free microstructure with a targeted and stable interstitial space is developed with balanced characteristics of high flux and high selectivity. Considering that the diffusion of a coagulant into a polymer solution is reciprocally proportional to the square of membrane thickness, reducing the outer layer dope flow rate can directly adjust the delayed demixing time lag (the time for the interface dense structure to evolve and densify before solidification), hence decreases the internal selective layer thickness and increases the flux tremendously. As expected,

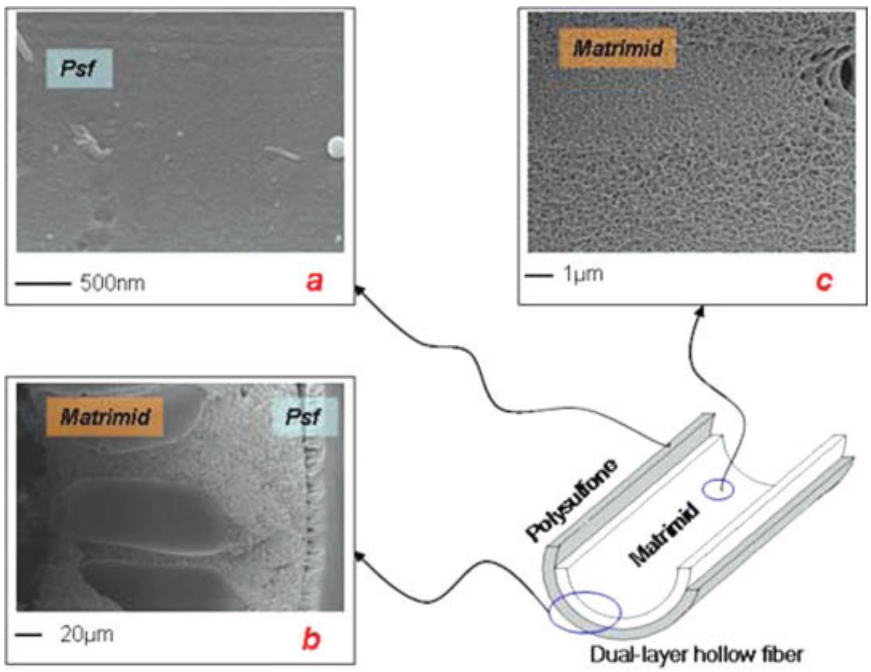

Figure 5. A typical FESEM pictures of Polysulfone/Matrimid dual-layer hollow fibers.

(a) Outer layer (Polysulfone) outer skin; (b) cross-section; (c) inner layer (Matrimid) inner skin. [Color figure can be viewed in the online issue, which is available at www.interscience.wiley.com.]

FESEM images in Figure 6 also show that the thickness of this layer is reduced from around 500 to 150 nm by reducing the PSf outer layer dope flow rate from 0.12 to 0.06 mL/min, where the corresponding flux (permeance) increases from 0.9 kg/m^2-h (permeance of 1.24 mol/m^2-h-kPa) to 3.9 kg/m^2-h (permeance of 5.41 mol/m^2-h-kPa). In addition, it is observed

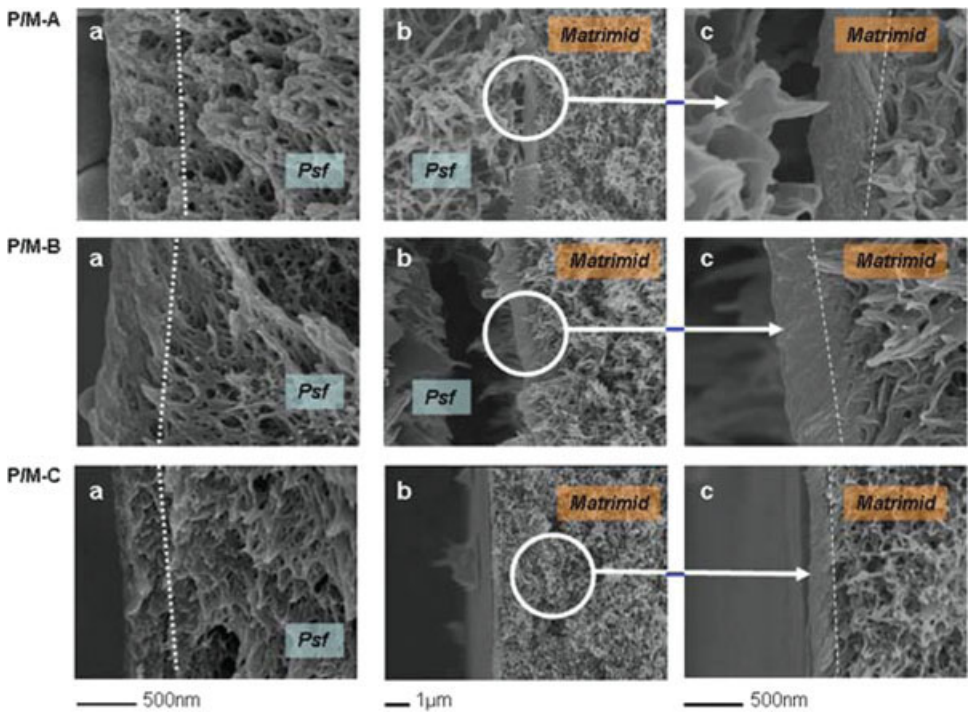

Figure 6. Cross-section morphology of Polysulfone/Matrimid dual-layer hollow fibers.

(a): Outer layer (Polysulfone) outer skin; (b, c): inner layer (Matrimid) outer skin. [Color figure can be viewed in the online issue, which is available at www.interscience.wiley.com.]

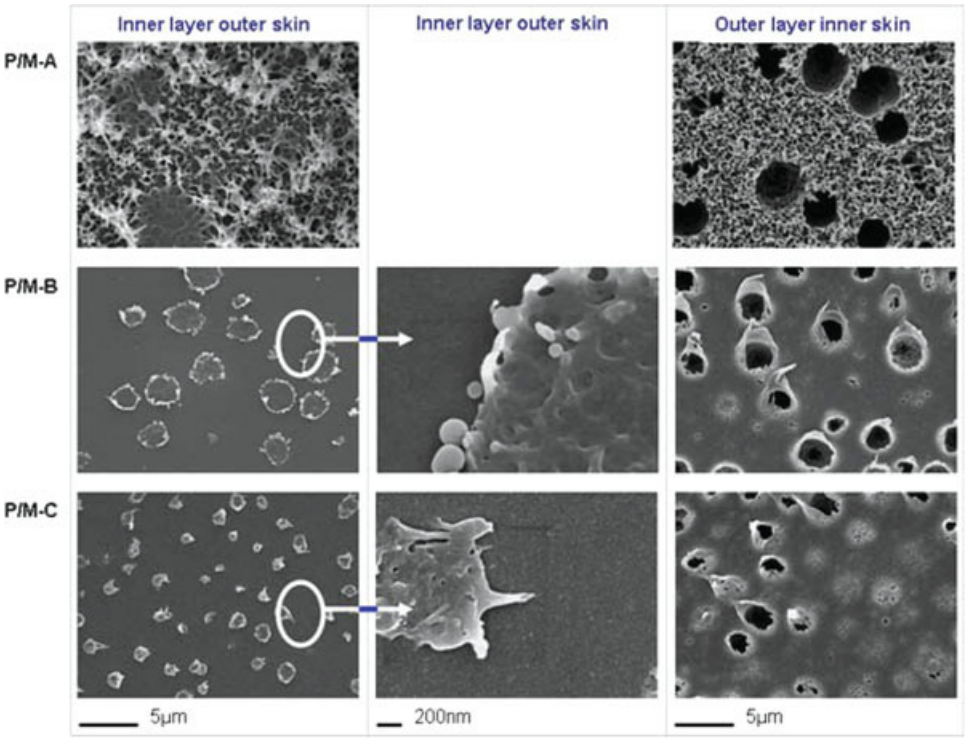

Figure 7. Morphology of interface skins of Polysulfone/Matrimid dual-layer hollow fiber.

[Color figure can be viewed in the online issue, which is available at www.interscience.wiley.com.]

obviously in Figure 6 that an ultrathin but defective PSf outer layer outer skin of less than 200 nm has been formed for the three fibers spun from different PSf dope flow rates. Additionally, the smaller the outer layer dope flow rate or the thinner the outer layer, the more defective the skin layer structure is. This is probably due to the fact that the significantly reduced shear-induced polymer chain orientation at the low PSf outer-layer flow rate may favor the defect formation.[25–27]

The interfacial surface morphologies of the PSf/Matrimid dual-layer hollow fiber are displayed in Figure 7. To observe the interface structure, the PSf outer layer has been peeled off from the inner layer using the method reported by Li et al.[28] As shown in the first row of Figure 7, the outer skin of the Matrimid inner layer of the fibers P/M-B and C have a dense and defect-free matrix with some round shape structures (diameter of $\sim$2–5μm) being evenly dispersed on it. The status of being dense and defect-free for above structure is more clearly confirmed by the second row of Figure 7 with a higher magnification (scale bar 200 nm). The inner skin of the PSf outer layer for the same fibers shown in the last row of Figure 7 is characterized of randomly distributed small pores and big holes. It is believed that the dispersed island structure on the Matrimid surface (the first row of Figure 9) is part of the inner skin of PSf outer layer (the third row) that has been tightly attached to the inner layer surface. The morphology of the fiber P/M-A is quite different from those of the other two hollow fibers. The top view of the Matrimid side shows completely porous structure, whereas the PSf side is also fully porous but tallies well with the Matrimid layer. Considering the cross-section morphology of well attached Matrimid and PSf layers in Figure 5 P/M-A(b), one possibility for this different morphology between PM-A and other two (PM/B and C) is that the two layers attachment of hollow fiber P/M-A is very strong because of the efficient interfacial diffusion, so that the weak point for structure breaking during the SEM sample preparation is located inside the PSf layer where comprising macrovoids as shown in Figure 5b.

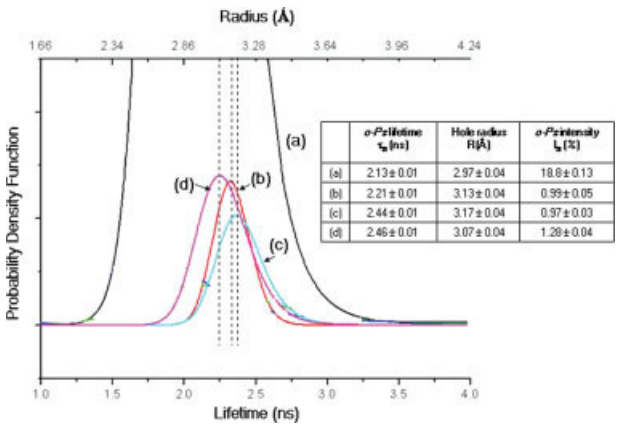

	o-Ps lifetime τ_3 (ns)	Hole radius R(Å)	o-Ps intensity I_3 (%)
(a)	2.13±0.01	2.97±0.04	18.8±0.13
(b)	2.21±0.01	3.13±0.04	0.99±0.05
(c)	2.44±0.01	3.17±0.04	0.97±0.03
(d)	2.46±0.01	3.07±0.04	1.28±0.04

Figure 8. Free-volume hole radius and distribution measured by positrumium annihilation lifetime spectroscopy (PALS).

(a) Neat Polysulfone dense membrane; (b) neat Matrimid dense membrane; (c) neat Matrimid hollow fiber; (d) Matrimid inner layer of Polysulfone/Matrimid dual-layer hollow fiber. [Color figure can be viewed in the online issue, which is available at www.interscience.wiley.com.]

Table 5. Elemental Analysis by X-ray Photoelectron Spectroscopy (XPS) of the Interface of Psf/Matrimid Dual-Layer Hollow Fiber

Polymer	Membrane		Mass Percentage (wt %) N_{1s}	S_{2p}
Polysulfone	Original (theoretical)		/	7.6
	Original (dense membrane)		/	6.0
	Dual-layer Polysulfone	*P/M-A*	1.1	6.4
	outer layer inner surface	*P/M-B*	1.2	6.2
		P/M-C	1.1	6.0
Matrimid	Original (theoretical)		5.3	/
	Original (dense membrane)		4	/
	Dual-layer Matrimid	*P/M-A*	3.2	2.0
	inner layer outer surface	*P/M-B*	4.5	1.1
		P/M-C	4.2	1.0

Based on the observed separation property and morphology together, it is concluded that the newly proposed approach synergistically combines the materials strengths of the two materials to produce excellent membrane for pervaporation via interfacial molecular diffusion driven by chemical potential and their miscibility characteristics. Therefore, with appropriate choices of a polymer pair and their solution formulations, one may be able to molecularly design high-performance hollow fiber membranes for biofuel separation with an ultrathin internal separation layer consisting of a miscible polymer blend with a targeted and stable interstitial space by means of dual-layer coextrusion.

PALS Characterization. To quantitatively elucidate the origins of selectivity enhancement, PALS was conducted on these membranes. Figure 8 shows their *ortho*-positronium lifetimes τ_3 and free-volume hole radius distributions. In general, the τ_3 value corresponds to the hole radius, the width of τ_3 is indicative of the distributions of free volume in polymeric systems.[29–31] The Matrimid material has a larger τ_3 and radius than the Psf material, and the τ_3 value of the Matrimid inner layer is smaller than both the neat Matrimid dense and hollow fiber membranes. The mean free-volume hole radii of the Matrimid inner layer, neat Matrimid dense and hollow fiber membranes are 3.07 ± 0.04, 3.13 ± 0.04, and 3.17 Å ± 0.04 Å, respectively. Because a tert-butanol molecule has an end-to-end distance, gyration radius and collision diameter of 4.35, 3.07, and 5.06 Å, respectively,[7,32] the Matrimid inner layer will have the highest diffusivity selectivity for tert-butanol dehydration because tert-butanol molecules have the lowest degree of freedom to diffuse through its pores compared with other two membranes. Therefore, the in-situ interfacial blending of Matrimid and Psf via dual-layer hollow fiber spinning not only overcomes the deficiencies of individual components but synergistically combines their strengths with ultrathin interfacial microstructure for biofuel separation.

Other Characterizations. To prove our hypothesis, XPS analyses was performed and Table 5 summarizes the elemental composition for the inner skin of the PSf outer layer and the outer skin of the Matrimid inner layer. The results show that N_{1s} (an element of Matrimid) and S_{2p} (an element of Psf) coexist in both inner and outer layer, strongly confirming the existence of intermolecular diffusion between the two solutions at the interface. This is further confirmed by EDX analysis results shown in Figure 9. A glass transition temperature (T_g) varying from 242 to 250°C for the present work was observed by differential scanning calorimetry (DSC) (Figure 10). This T_g is between the T_g*s* of Psf (186°C) and Matrimid (320°C), which is indicative of the existence of a miscible blend at the interface. The composition of possible blending calculated based on Fox equation (shown in Figure 10)[33] are 0.45/0.55 to 0.38/0.62 of Psf/Matrimid (weight ratio). Fourier transform infrared (FTIR) spectra in Figure 11 display wavelength shifts of the imide C=O group (from 1715 to 1719 cm^{-1}), and the C—N—C group (from 1092 to 1098 cm^{-1}) because of molecular interactions.

The X-ray diffraction (XRD) patterns of the neat Matrimid and Psf flat dense and single-layer hollow fiber membranes as well as the Matrimid inner layer of dual-layer hollow fibers are displayed in Figure 12. The Matrimid and Psf flat dense membranes show diffraction peaks at Bragg angles (2θ) of 15.7° and 18.2°, corresponding to d-spaces of 5.63 and 4.87 Å, respectively. These observations suggest a smaller interstitial space among polymeric chains of Psf than Matrimid. Figure 12 also reveals that the peak intensity of Matrimid inner layer of dual-layer hollow fiber is higher than that of neat Matrimid single-layer. The neat Matrimid single-layer hollow fiber has an apparent shoulder peak (highlighted in the circle) implying some structure of smaller interchain distance, whereas the shoulder for the Matrimid inner layer is quite obscure. Qualitatively, these changes suggest a higher degree of chain packing in the Matrimid inner layer

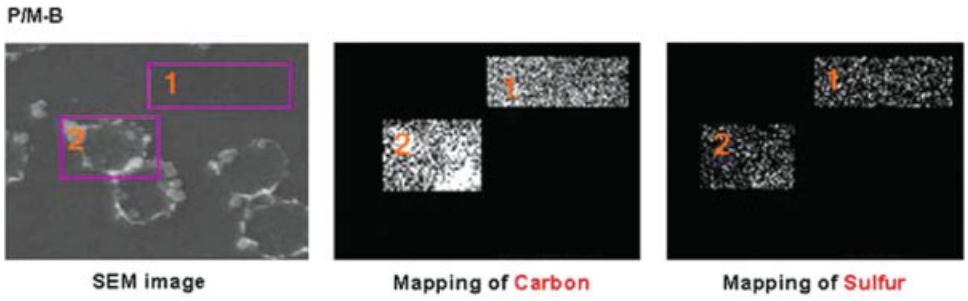

Figure 9. Energy dispersive spectroscopy (EDX) mapping of the Matrimid inner layer outer surface of the Polysulfone/Matrimid dual-layer hollow fibers (1 and 2 represent different morphologies of the membranes).

[Color figure can be viewed in the online issue, which is available at www.interscience.wiley.com.]

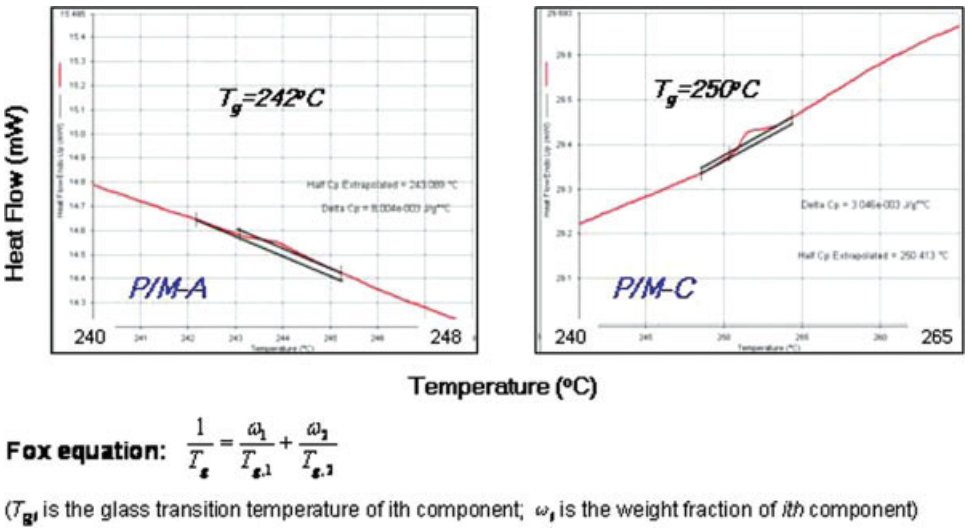

Figure 10. Differential scanning calorimetry (DSC) curve (1st heating cycles) indicating the possible blending at the interface of the Polysulfone/Matrimid dual-layer hollow fibers (N2 flow rate: 20 mL/min; heating rate: 20 °C/min).

[Color figure can be viewed in the online issue, which is available at www.interscience.wiley.com.]

because of the delayed demixing before solidification and the interference from Psf molecules with a smaller interstitial space.

Effect of feed composition on PSf/Matrimid dual-layer hollow fiber performance

Figure 13 shows the PSf/Matrimid dual-layer hollow fiber performance in flux and separation factor with varied feed compositions while maintaining the feed temperature at 80°C; Figure 14 shows the performance in permeance and selectivity. The performance patterns of the fibers P/M-A to C as a function of water composition have no fundamental differences. As shown in the Figure 13A, the order of total flux for the PSf/Matrimid hollow fibers has the following sequence, which is hollow fiber P/M-C > P/M-B > P/M-A, throughout the whole feed water concentration; the order of the separation factor is just opposite. Further observation of Figure 13A reveals that all the total flux increases with an increase in water concentration in the feed from 10 to 70 wt %; the total flux increase is mainly because of the increase of water flux as shown in Figure 13B. There is no obvious trend observed of tert-butanol flux. Figure 13B also exhibits that the separation factor drops seriously over the same water concentration range.

When we convert the results into permeance and selectivity as shown in Figure 14, the curves of permeance plotted as a function of feed composition exhibit almost the same

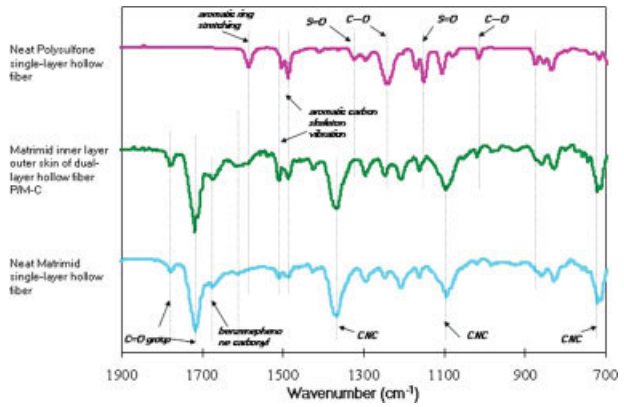

Figure 11. Comparison of fourier-transformed infrared spectroscopy (FTIR) curves of Polysulfone/Matrimid dual-layer and Polysulfone single-layer hollow fibers.

[Color figure can be viewed in the online issue, which is available at www.interscience.wiley.com.]

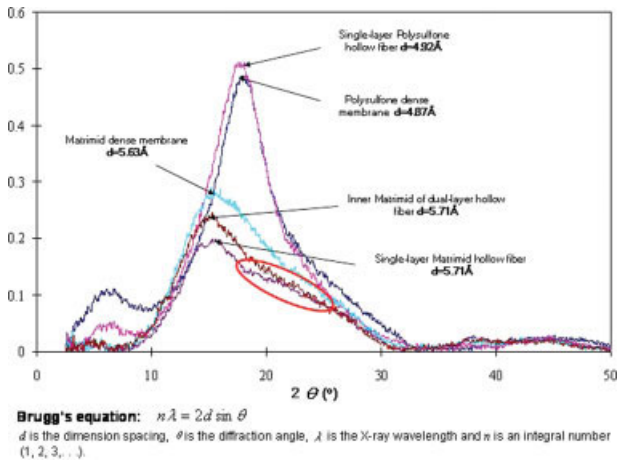

Figure 12. X-ray diffraction (XRD) patterns of dense membranes and single-layer hollow fibers from neat Polysulfone and Matrimid and Polysulfone/Matrimid dual-layer hollow fibers.

[Color figure can be viewed in the online issue, which is available at www.interscience.wiley.com.]

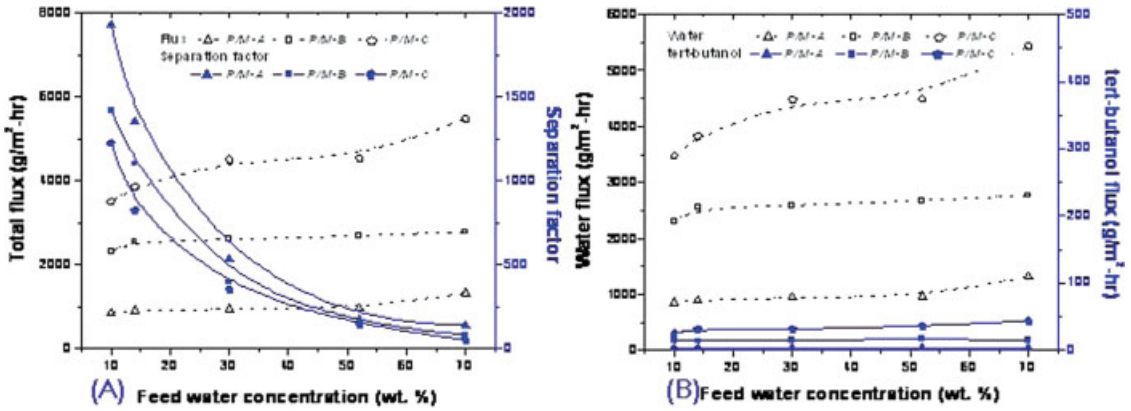

Figure 13. Water and tert-butanol flux and separation factor of Polysulfone/Matrimid dual-layer hollow fibers as a function of feed composition.

Feed: tert-butanol/water; final temperature: 80 °C; flow rate of feed mixture 30 L/h per module. [Color figure can be viewed in the online issue, which is available at www.interscience.wiley.com.]

patterns as flux in Figure 13. Even though selectivity also varied in the same pattern as separation factor, the change is only in a minor degree. For example, the separation factor for hollow fiber P/M-C decreases from 1200 to only 52, when feed water concentration increase from 10 to 70 wt %; while, the selectivity was only reduced from 1000 to 680. This distinction between the separation factor and selectivity mainly attributes to the decoupling of the effect of processing parameters on the performance evaluation as proved by previous researches. It is generally accepted that permeance and selectivity represent more accurate permeant-specific intrinsic membrane properties.

Generally, the dependence of polymeric membrane performance in pervaporation dehydration is determined by the degree of hydrophilicity of the membrane material. But the some conditions related to the PSf/Matrimid dual-layer hollow fibers in this study make the situation complicated. First, both the PSf and Matrimid with different solubility parameters (or hydrophilicity) will react to the feed composition simultaneously. Second, the performance of the individual layers will follow a resistance model to give the overall performance of dual-layer hollow fibers.[34] Furthermore, since the most selective layer located at the interface, concentration polarization and pressure loss inside PSf outer layer may occur.[35,36] Nevertheless, the properties of permeance and selectivity in Figure 14 suggest that these hollow fibers have quite stable performance within a wide range of water concentration on a whole.

Conclusions

In conclusion, this work has demonstrated a novel molecular engineering and membrane fabrication that can synergistically produce polymeric membranes exhibiting separation performance approaching ceramic membranes. The newly discovered membranes are fabricated by dual-layer coextrusion technology in just one step through phase inversion. An ultrathin dense-selective layer made of a miscible blend with a targeted and stable interstitial space is formed at the interface of two layers for biofuel separation. The combined

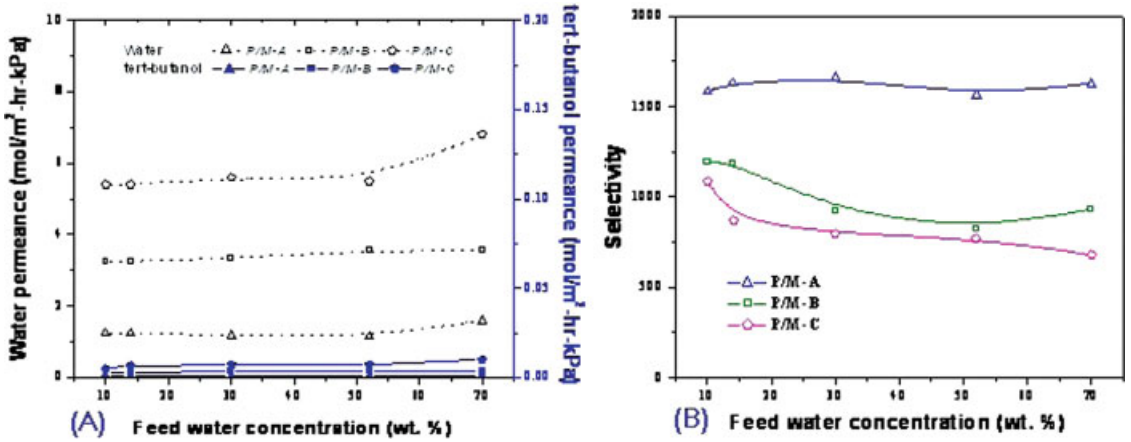

Figure 14. Water and tert-butanol permeance and selectivity of dual-layer hollow fibers as a function of feed composition.

Feed: tert-butanol/water; final temperature: 80 °C; flow rate of feed mixture: 30 L/h per module. [Color figure can be viewed in the online issue, which is available at www.interscience.wiley.com.]

molecular engineering and membrane fabrication approach may revolutionize future membrane research and development for purification and separation in energy, environment, and pharmaceuticals.

Acknowledgments

The authors thank Ms. Yan Wang for DSC characterization, Dr. Youchang Xiao for XPS characterization, and Mr. Panu Sukipaneenit for reference search. They also thank A-Star and NUS for funding this research with the grant numbers of R-398-000-029-305, R-398-000-044-305, and R-279-000-184-112.

Literature Cited

1. Koonin SE. Getting serious about biofuel. *Science*. 2006;311:435–435.
2. Ragauskas AJ, Williams CK, Davison BH, Britovsek G, Cairney J, Eckert CA Jr, Frederick WJ, Hallett JP, Leak DJ, Liotta CL, Mielenz JR, Murphy R, Templer R, Tschaplinski T. The path forward for biofuels and biomaterials. *Science*. 2006;311:484–489.
3. Yampolskii Y, Pinnau I, Freeman BD. *Materials Science of Membranes for Gas and Vapor Separation*. New York: Wiley, 2005.
4. Peters TA, Fontalvo J, Vorstman MAG, Benes NE, van Dam RA, Vroon ZAEP, van Soest-Vereammen ELJ, Keurentjes JTF. Hollow fiber microporous silica membranes for gas separation and pervaporation. *J Membr Sci*. 2005;248:73–80.
5. Gallego-Lizon T, Edwards E, Lobiundo G, Freitas dos Santos L. Dehydration of water/tert-butanol mixtures by pervaporation: comparative study of commercially available polymeric, microporous silica and zeolite membranes. *J Membr Sci*. 2002;197:309–319.
6. Guo WF, Chung TS, Matsuura T, Wang R, Liu Y. Pervaporation study of water and tert-butanol mixtures. *J Appl Polym Sci*. 2004;91:4082–4090.
7. Qiao XY, Chung TS, Guo WF, Matsuura T, Teoh MM. Dehydration of isopropanol and its comparison with dehydration of butanol isomers from thermodynamic and molecular aspects. *J Membr Sci*. 2005;252:37–49.
8. Kleiner K. Civil aviation faces green challenge. *Nature*. 2007;448:120–121.
9. Wijmans JG, Baker RW. The solution-diffusion model: a review. *J Membr Sci*. 1995;107:1–21.
10. Feng X, Huang RYM. Liquid separation by membrane pervaporation: a review. *Ind Eng Chem Res*. 1997;36:1048–1066.
11. Barton AFM. *CRC Handbook of Solubility Parameters and Other Cohesion Parameters*. Boca Raton, FL: CRC press, 1985.
12. Matsura T. *Synthetic Membrane and Membrane Separation Process*. Boca Raton, NY: CRC press, 1995.
13. Friedrich C, Drakoncourt A, Nole C, Monnerie L. Asymmetric reverse osmosis and ulfiltration membrane prepared from sulfonated polysulfone, desalination. 1981;36:39–62.
14. Wang KY, Chung TS, Rajagopalan R. Dehydration of tetrafluoropropanol (TFP) by pervaporation via novel PBI/BTDA-TDI/MDI copolyimide (P84) dual-layer hollow fiber membranes. *J Membr Sci*. 2007;287:60–66.
15. Wijams JG, Baker RW. A simple predictive treatment of the permeation process in pervaporation. *J Membr Sci*. 1993;79:101–113.
16. Wijams JG. Process performance = membrane properties +operating conditions. *J Membr Sci*. 2003;220:1–3.
17. Qin Y, Sheth JP, Sirkar KK. Pervaporation membranes that are highly selective for acetic acid over water. *Ind Eng Chem Res*. 2003;42:582–595.
18. Tsai HA, Chen HC, Chou WL, Lee KR, Yang MC, Lai JY. Pervaporation of water/alcohol mixtures through chitosan/cellulose acetate composite hollow-fiber membranes. *J Appl Polym Sci*. 2004;94:1562–1568.
19. Tsai HA, Ciou YS, Hu CC, Lee KR, Yu DG, Lai JY. Heat-treatment effect on the morphology and pervaporation performances of asymmetric PAN hollow fiber membranes. *J Membr Sci*. 2005;255:33–47.
20. Liu RX, Qiao XY, Chung TS. The development of high performance 84 co-polyimide hollow fibers for pervaporation dehydration of isopropanol. *Chem Eng Sci*. 2005;60:6658–6673.
21. Zhou FB, Koros WJ. Study of thermal annealing on Matrimid fiber performance in pervaporation of acetic acid and water mixtures. *Polymer*. 2006;47:280–288.
22. Dong YC, Zhang L, Shen JN, Chen HL. Preparation of poly (vinyl alcohol)-sodium alginate hollow fiber composite membranes and pervaporation dehydration characterization of aqueous alcohol mixtures. *Desalination*. 2006;193:202–210.
23. Liu RX, Qiao XY, Chung TS. Dual-layer P84/polyethersulfone hollow fibers for pervaporation dehydration of isopropanol. *J Membr Sci*. 2007;294:103–114.
24. Teoh MM, Chung TS, Wang KY, Guiver MD. Torlon/P84 co-polyamide-imide blended hollow fibers and their chemical cross-linking modifications for pervaporation dehydration of isopropanol. *Sep Sci Tech*. 2008;61:404–413.
25. Cao C, Chung TS, Chen SB, Dong ZJ. The study of elongation and shear rates in spinning process and its effect on gas separation performance of poly(ether sulfone) (PES) hollow fiber membranes. *Chem Eng Sci*. 2004;59:1053–1062.
26. Peng N, Chung TS, Wang KY. Macrovoid evolution and critical factors to form macrovoid-free hollow fiber membranes. *J Membr Sci*. 2008;318:363–372.
27. Widjojo N, Chung TS. Thickness and air gap dependence of macrovoid evolution in phase-inversion asymmetric hollow fiber membranes. *Ind Eng Chem Res*. 2006;45:7618–7626.
28. Li DF, Chung TS, Wang R. Morphological aspects and structure control of dual-layer asymmetric hollow fiber membranes formed by a simultaneous co-extrusion approach. *J Membr Sci*. 2004;243:155–175.
29. Jean YC, Mallon PE, Schrader DM. *Principles and Applications of Positron and Psitronium Chemistry*. Singapore: World Science Publications, 2003.
30. Tin PS, Chung TS, Hill AJ. Advanced fabrication of carbon molecular sieve membranes by non-solvent pretreatment of precursor polymers. *Ind Eng Chem Res*. 2004;43:6476–6483.
31. Park HB, Jung CH, Lee YM, Hill AJ, Pas SJ, Mudie ST, Wagner EV, Freeman BD, Cookson DJ. Polymers with cavities tuned for fast selective transport of small molecules and ions. *Science*. 2007;318:254–258.
32. van Leeuwen ME. Derivation of stockmayer potential parameters for polar fluids. *Fluid Phase Equilib*. 1994;99:1–18.
33. Chung TS, Foley P, Jaffe M. Ternary fluoro-containing polyimide blends and fluoro-containing polyimide/polyester blends. *Polym Adv Technol*. 1997;8:537–544.
34. Huang RYM, Feng X. Resistance model approach to asymmetric polyetherimide membranes for pervaporation of isopropanol/water mixtures. *J Membr Sci*. 1993;84:15–27.
35. Koops GH, Nolten JAM, Mulder MHV, van den Boomgaard T, Smolders CA. Integrally skinned polysulfone hollow fiber membranes for pervaporation. *J Apply Polym Sci*. 1994;54:384–404.
36. Matsuura T. *Synthetic Membranes and Membrane Separation Processes*. Boca Raton: CRC Press, 1994.

Manuscript received Apr. 22, 2008, and revision received July 27, 2008.